Letters in Applied NanoBioScience
Open-Access Journal (ISSN: 2284-6808)

Article
Volume 12, Issue 4, 2023, 153
https://doi.org/10.33263/LIANBS124.153

Effect of Copper Nanoparticle Contents in Polyaniline/ Copper Nanoparticle (PANi/CuNPs) Composites Photoanode Material on the Photovoltaic Performance of Organic Solar Cells

Surajudeen Otolowo Azeez [1], Kamaldeen Olasunkanmi Suleman [2,*], Akeem Adekunle Adewale [1], Nurudeen Kolawole Olasunkanmi [1], Yekinni Kolawole Sanusi [3,*], Sarafadeen Ayinde Azeez [4]

[1] Department of Physics, College of Pure and Applied Science Kwara State University, Malete, Nigeria; soazeez81@student.lautech.edu.ng (S.O.A.); adewaleakeem12@gmail.com (A.A.A.); nurudeen.olasunkanmi@kwasu.edu.ng (N.K.O.);
[2] Department of Physics, School of Basic Sciences, Nigeria Maritime University Okerenkoko, Delta State, Nigeria; kamaldeen.suleman@nmu.edu.ng (K.O.S.);
[3] Department of Pure and Applied Physics, Ladoke Akintola University of Technology, Nigeria; yksanusi@lautech.edu.ng (Y.K.S.);
[4] Department of Mechanical Engineering, Usmanu Danfodiyo University, Sokoto, Nigeria; otolowo2016@gmail.com (S.A.A.);
* Correspondence: kosuleman@lautech.edu.ng (K.O.S.);

Scopus Author ID 57219509791

Received: 9.06.2022; Accepted: 5.07.2022; Published: 18.11.2022

Abstract: Scientists have embraced the green synthesis method for nanoparticle synthesis because of its many advantages over physical and chemical methods. It does not release harmful chemicals and is an economically cheap process. As a result, the present study synthesized copper nanoparticles (CuNPs) from siam leaf (*Chromolaena odorata*) extract. The synthesized CuNPs were used to prepare polyaniline/copper nanocomposites (PANi/CuNPs) which were then used as a photoanode in the solar cell. The structural, morphological, and optical properties of the synthesized CuNPs were characterized by Fourier Transform Infrared Spectroscopy (FTIR), Atomic Force Microscopy (AFM), UV–Visible spectroscopy, Scanning Electron Microscopy (SEM), and X-Ray Diffraction (XRD). The XRD pattern revealed a crystalline nature for CuNPs, with the average diameter of particles being 20 µm. SEM analysis revealed a spherical shape with a size ranging from 10 to 30 µm. The solar cell fabricated with PANI/40%CuNP as a photoactive anode layer designates an overall efficiency of 19.2 % with a sheet resistance of 0.248 Ω. This performance was higher than PANI-based solar cells, with an efficiency of 16.5 % and sheat resistance of 5.07 Ω under similar conditions. The synthesized CuNPs show commendable potential for application in solar cell fabrication. Thus, this work provides further insight into improvement in the efficiency of organic solar cells.

Keywords: green synthesis; copper nanoparticles; polyaniline; X-ray diffraction; photoanode.

1. Introduction

Conventional energy sources, including fossil fuels, have associated drawbacks, including environmental pollution and depletion of resources. Consequently, in order to reach sustainable development and a clean environment, it is often advised to use renewable energies. Due to its wide availability worldwide [1–3], solar energy is the most interesting type of

renewable energy commonly considered. Developing efficient and cost-effective solar cells is one of the most important challenges in solar technology and research.

Generally, photovoltaic solar cells are often classified as either organic solar cells or thin-film organic solar cells. Inorganic (commonly known as Silicon (Si)) solar cells is still the most common in the photovoltaic market owing to a combination of high stability, long lifespan, and higher efficiency (15–20 %) [4,5]. The foremost inadequacies associated with Si solar cells include inflexibility, purity of Si, high energy processing, and loss of efficiency at elevated temperatures [6]. Owing to these, researchers are now developing new light-sensitive organic materials for solar cell applications. Organic light-sensitive materials have been classified into perovskites, donor/acceptor polymers, and photo-sensitizers. By varying the synthesis conditions, these light-sensitive materials' electronic and optical properties can easily be altered [7]. From previous studies, Perovskite solar cells (PVSCs) have the highest power conversion efficiency (PCE). For example, a PCE of 21.3 % has been recorded for single-junction architecture PVSCs [8]. However, the commercialization of PVSCs is facing several obstacles: poor stability against oxygen and humidity [9–11] and the complex fabrication process [12]. Contrastingly, dye-sensitized solar cells (DSSCs) have the advantage of ease of fabrication and have efficiency as high as 14 % [13–17]. DSSCs, unlike others, can work in dispersed sunlight and dull environments [18]. In spite of all these advantages, the major shortcoming is that the lifetime and PCE of DSSCs are far less than Si solar cells [19–27]. Hence, to improve and make this technology more viable, there is a need for further research and development.

Several methods are used to synthesize nanoparticles [28–31]. The problem associated with these physical methods is that, in addition to requiring a lot of time to achieve thermal stability, they consume a lot of energy while raising the environmental temperature around the source material [32]. Chemical synthesis, which is an advantage of producing high PCEs, is limited by its use of toxic solvents and chemicals harmful to our already toxic and suffering environment [33,34]. Owing to these highlighted shortcomings, biological synthesis is a better alternative for generating nanoparticles and is usually preferred over physical and chemical synthesis methods [35].

This work used plant-assisted reduction to synthesize polyaniline/copper nanoparticles (PANi/CuNP) composites. Here, we studied and investigated the morphological, structural, optical, and electrical characteristics of PANi/CuNP composites. The synthesized materials were employed as photoactive anode materials for photovoltaic applications. The results of this study suggest that PANi/CuNP composites could be used as an alternative to pure PANi material for the large-scale production of solar cells.

2. Materials and Methods

2.1. Materials.

Chromolaena odorata plants (siam flowers) were collected around the campus of the Kwara State University (KWASU), Malete, Kwara State, Nigeria. Copper Sulphate Pentahydrate (99 % purity) was purchased from Malaysia. As a result, these chemicals were used without further purification. Before usage, all glasswares were initially washed with a freshly prepared Piranha etch, followed by deionized water of 18.2 MΩ.cm resistivities, after which they were dried in the oven. For the collection of extract, Whatman filter paper grade-I was used. Deionized distilled water was used for the entire duration of the experiment.

2.2. Methods.

2.2.1. Preparation *Chromolaena odorata* leaf extract.

Chromolaena odorata leaves (siam flowers) were collected around the campus of Kwara State University, Malete. The leaves were rinsed and washed with deionized water to remove impurities and then sun-dried to remove all the moisture. 35 g of the dried leaves was grinded in a pestle and mortar to obtain a fine powder. The powdered leaf was boiled in 100 ml deionized water for about 2 hr at 60 °C until the water turned green and continuously until the green color changed to brown, as shown in Figure 1a. it was then allowed to cool for 10-15 mins at room temperature. While the residue was discarded, the plant extract was collected as filtrate in a beaker through Whatman filter paper. Pending subsequent usage, the aqueous extract was stored at room temperature (Figure 1b).

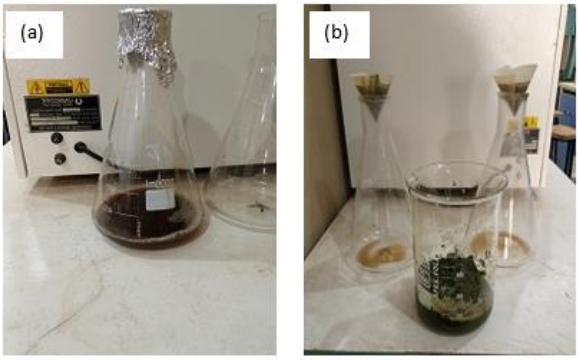

Figure 1. *Chromolaena odorata* leaf extract.

2.2.2. Green synthesis of copper nanoparticles.

A solution of 0.1 M Copper Sulphate ($CuSO_4.5H_2O$) was prepared in deionized water. The mixture was stirred on a magnetic stirrer at room temperature to dissolve the zinc nitrate powder completely. Afterward, 30 mL of the aqueous leaf extract was gradually added to 100 mL of the prepared copper sulfate solution. The mixture was then heated and stirred on a hot plate for 3-4 hrs at 60 °C until a jelly paste was formed. The jelly product was calcinated in a furnace at 400 °C for 3-4 hrs. After calcination, Copper Nanoparticles (CuNPs) were obtained in brownish powder form, as shown in Figure 2.

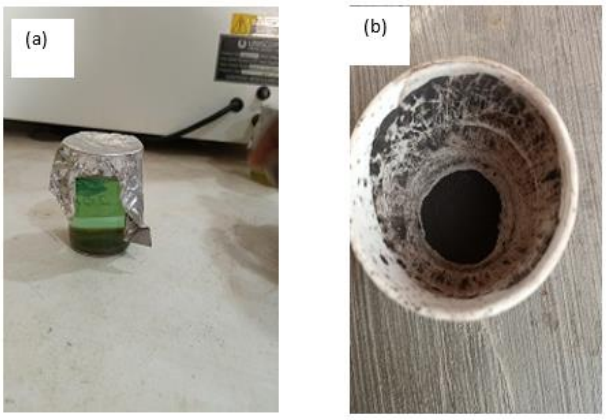

Figure 2. Precipitated CuNPs and CuNPs in powdered form.

2.2.3. Preparation of copper/polymer nanocomposite.

A weighed amount of Copper nanoparticles were dispersed in 5 mL of deionized water, and 0.5 g of polyaniline (PANI) was added. The mixture was diffused for 1 hr using a sonicator at room temperature. In this way, Copper-Polyaniline nanocomposite was prepared. However, this preparation was repeated for different ratios of the weighed amount of copper nanoparticles that is 1:1, 1:0.8, 1:0.6, 1:0.4, and 1:0.2, respectively, to select the best mixing ratio. The obtained polymer composite was filtered and washed with deionized water.

2.2.4. Characterisation of copper nanoparticles.

The prepared nanoparticles were characterized structurally, optically and morphologically via X-ray Diffraction, UV–Visible Spectrophotometer, Fourier transform infrared spectroscopy (FTIR, Bruker vertex 70, Germany), and Scanning Electron Microscopy (SEM), respectively. Finally, the prepared PANi/CuNPs were studied for photovoltaic applications.

3. Results and Discussion

3.1. X-ray diffraction analysis.

The CuNPs were characterized using XRD-D8 Advance Bruker AXS. Figure 3 shows the x-ray diffraction analysis pattern of the CuNPs in powder form. The analysis was done for angles ranging from 25º to 75º. Three conspicuous diffraction peaks occurred at Bragg's angles 43.37°, 53.53°, and 74.12°, corresponding to the planes (111), (200), and (220), respectively. The XRD pattern revealed the orientation and crystalline structure of CuNPs. For phase speciation, the XRD pattern was compared with ICDD reference data for Copper. This confirms a successful synthesis of CuNPs by the green synthesis method and the formation of crystalline and wurtzite hexagonal structures. The crystallite size (D) of the CuNPs was calculated from the highest peak (111) in the XRD graph using the Scherrer equation [36,37]:

$$D = \frac{0.9\lambda}{\beta \cos\theta} \quad (1)$$

where λ is the x-ray wavelength, $\theta =$ the Bragg diffraction angle, $\beta =$ the FWHM of the peak appearing at the diffraction angle.

The average particle diameter of CuNPs was found to be 20 µm. The phase purity of CuNPs is confirmed as no diffraction peaks of other phases are detected.

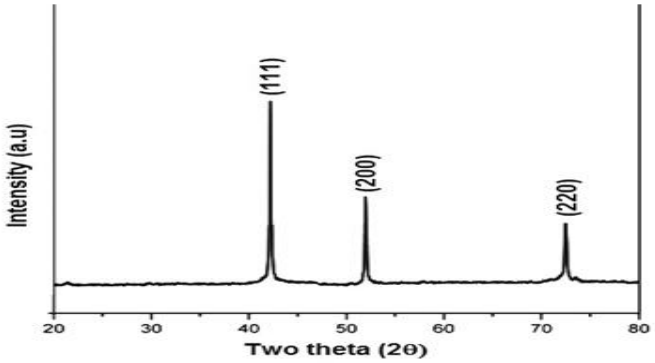

Figure 3. XRD spectrum of PANi/CuNP composites.

3.2. SEM analysis.

The particle dimensions and morphology of the synthesized CuNP, PANi, and PANi/CuNP composites were examined by scanning electron Microscope (SEM) MIRA3-TESCAN. Figure 4 (a, b, and c) show the SEM images of these materials. These images showed clearly that the particles are in nanostructure form. In Figure 4 (a), it was revealed that copper nanoparticle powders are composed of non-agglomerated random-shaped particles, which tend to build and aggregate to form a flower-shaped structure. In Figure 4 (b), the SEM image of PANi shows a crystalline structure and cluster each other. Lastly, in Figure 4 (c), PANi/CuNP composite show a higher tendency of agglomerations owing to the close relation interface movement of electron and holes, which are very important for high efficiency in hybrid solar cells. The average particle diameter was estimated as 20 µm, which corresponds to the XRD result. These results confirmed the strong incorporation of copper metal in the polymer matrix, which is proof of good photovoltaic performance properties, as reported by [38].

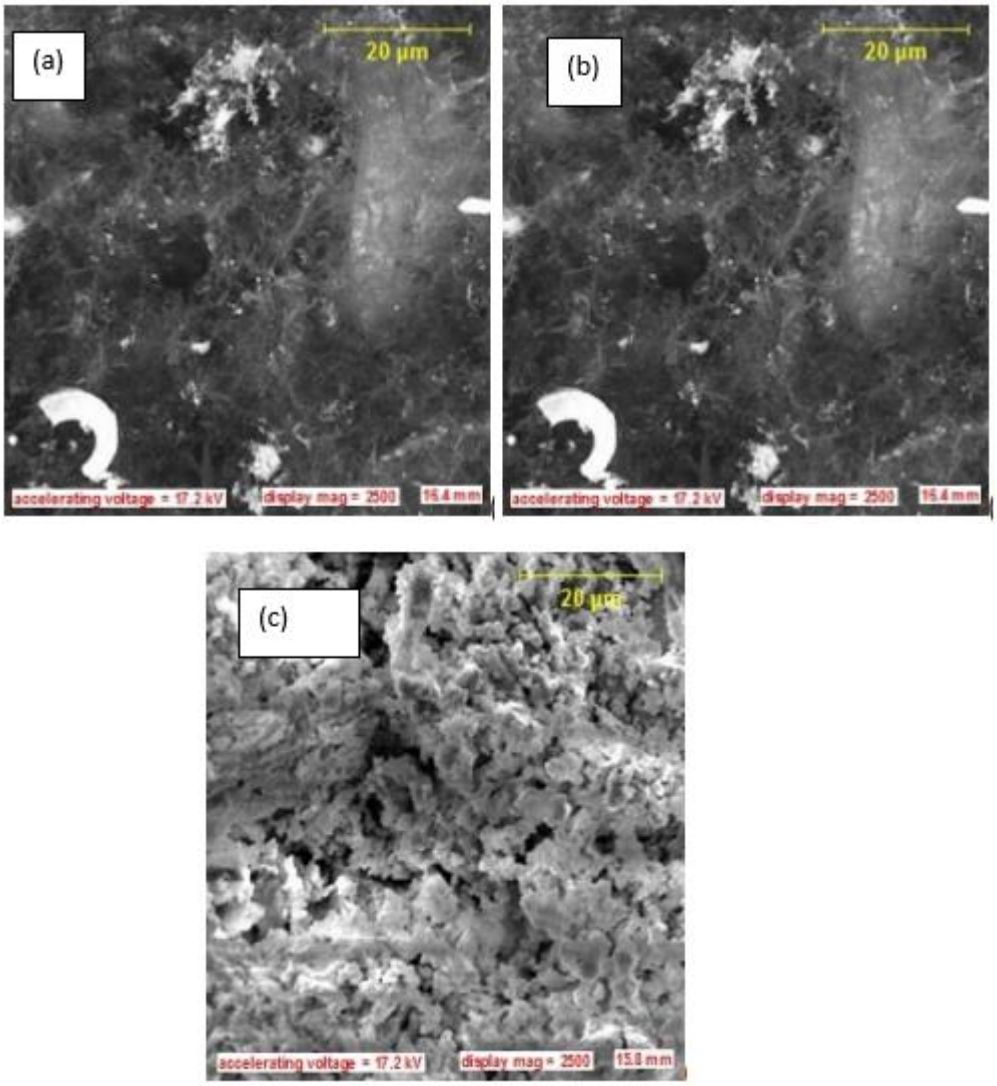

Figure 4. SEM images of (a) CuNP (b) PANi, and (c) PANi/CuNP.

3.3. AFM analysis.

In this examination, the assessment of PANi, CuNPs, and PANi/CuNPs were done through AFM strategy. The particles of the materials were broken down by Atomic Force Microscopy (AFM) for point-by-point size and morphology analysis. The three-dimensional

(3D) surface morphology and size examinations obtained from AFM are shown in Figure 5. In Figure 5(a), CuNPs show a gravel-like structure with the dimension of scanning area 3.12 um × 3.12 um. An infinitesimal-like structure with a dimension of 12.6 um × 12.6 was observed in PANi material, as presented in Figure 5(b). Meanwhile, the morphology of PANi/CuNPs nanocomposite in Figure 4.8(c) shows layer by layer arrangement

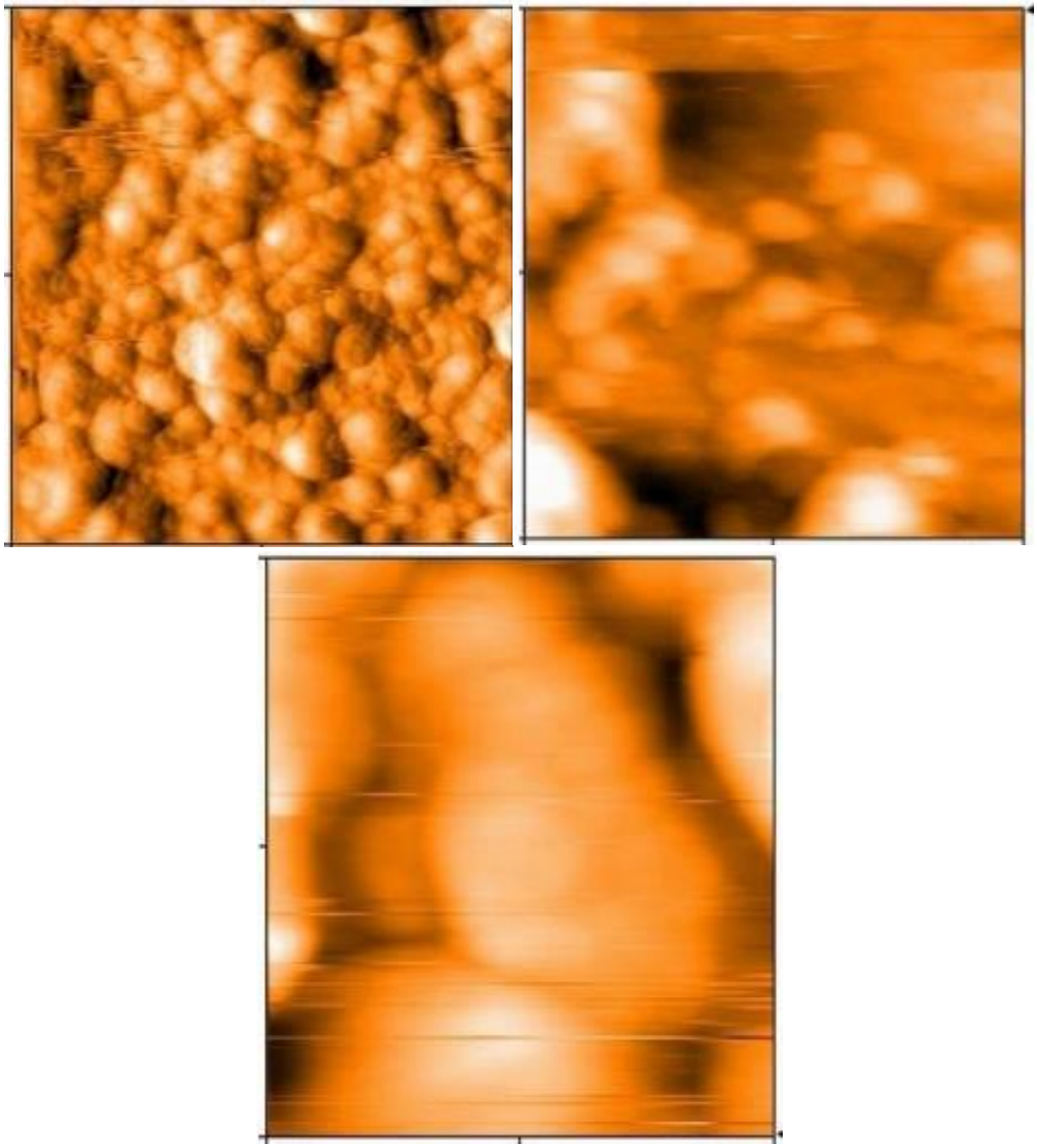

Figure 5. AFM images of (a) Copper nanoparticle, (b) Polymer, and (c) Copper/Polymer.

3.4. FT-IR analysis.

FT-IR spectrum of green synthesized CuNPs done using a Bruker Alpha FTIR spectrometer is shown in Figure 6. The spectral peaks at 1056 cm^{-1} were attributed to N–H stretching. The peak around 2936 cm^{-1} was adjudged to be due to C–H stretch. The peak at 835 cm^{-1} and 613 cm^{-1} is indicative of alkynes and alkyl halides. The strong vibrational bands at 3500 cm^{-1} were assigned to the stretching modes for forming CuNPs.

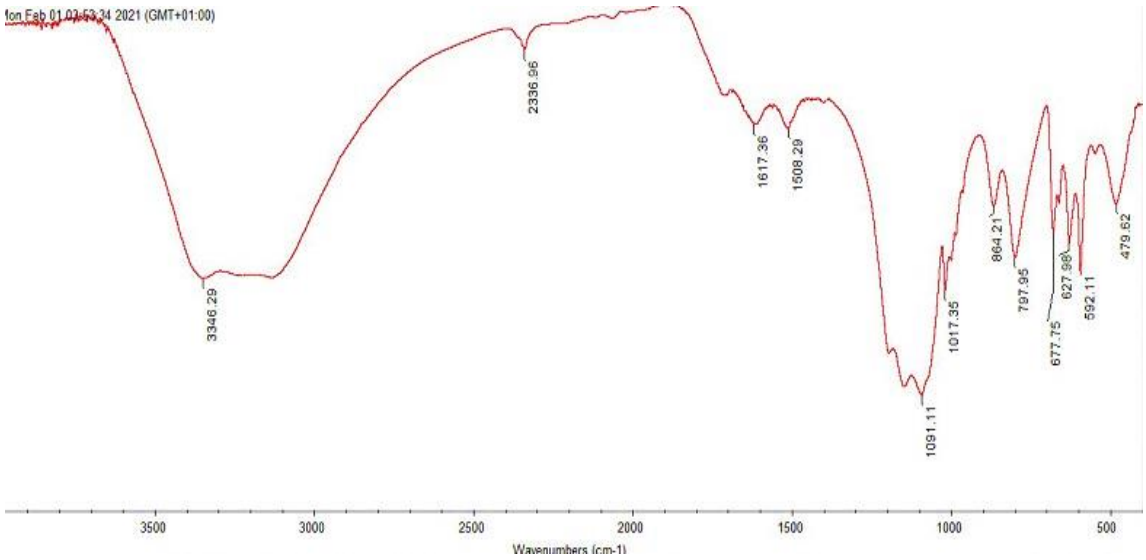

Figure 6. FT-IR Spectrum of synthesized CuNPs.

3.4. Optical properties.

The optical properties of PANi/CuNP film-based-photoactive anode layer devices were studied considering the effect of copper/polyaniline mixing ratio, spin coating speed (film thickness), annealing temperature, and time.

A photon wavelength range of 350-1100 nm was considered in this work. As shown in Figure 7, the absorption spectrum revealed intense absorption in the ultraviolet band of about 300 - 350 nm for all samples of the different materials. The highest absorbance was recorded for PANi/CuNP with a mixing ratio of 1:0.4 at a spin coating speed of 1000 rpm. The absorption spectrum revealed a shift in the absorption peak due to charge transfer transitions within PANi/CuNP nanocomposites.

For the best mixing ratio, the annealing temperature was varied with time to determine the optimal annealing temperature for the fabricated copper/polymer composite film photoactive layer device. The leverage of thermal annealing temperature on the UV-Vis absorption was investigated at different temperatures ranging from 100°Cto 400°C. Generally, the thermal annealing gives the device high-quality film and enhances the crystallinity of PANi/CuNP composite based-photoactive layer. This, in turn, improves the performance conversion efficiency by increasing the photogenerated electrons transmitted to the photoactive layer, thereby improving the performance of the polymer solar cell.

As shown in Figure 8, it was deduced that the annealing temperature for the maximum absorbance and good conversion performance is 400°C for 30 minutes. The film annealed at 400°C gave better optical properties due to the high refractive index [39].

The absorption coefficient (α) and the optical band gap (E_g) were determined by equations [40–42]

$$\alpha = 2.303\left(\frac{A}{t}\right) \quad (2)$$

$$(\alpha h\nu) = D\left(h\nu - E_g\right)^n \quad (3)$$

where;

A: absorbance, t: thickness of the sample, D: is a constant. (n): exponent that is dependent on the type of optical transition.

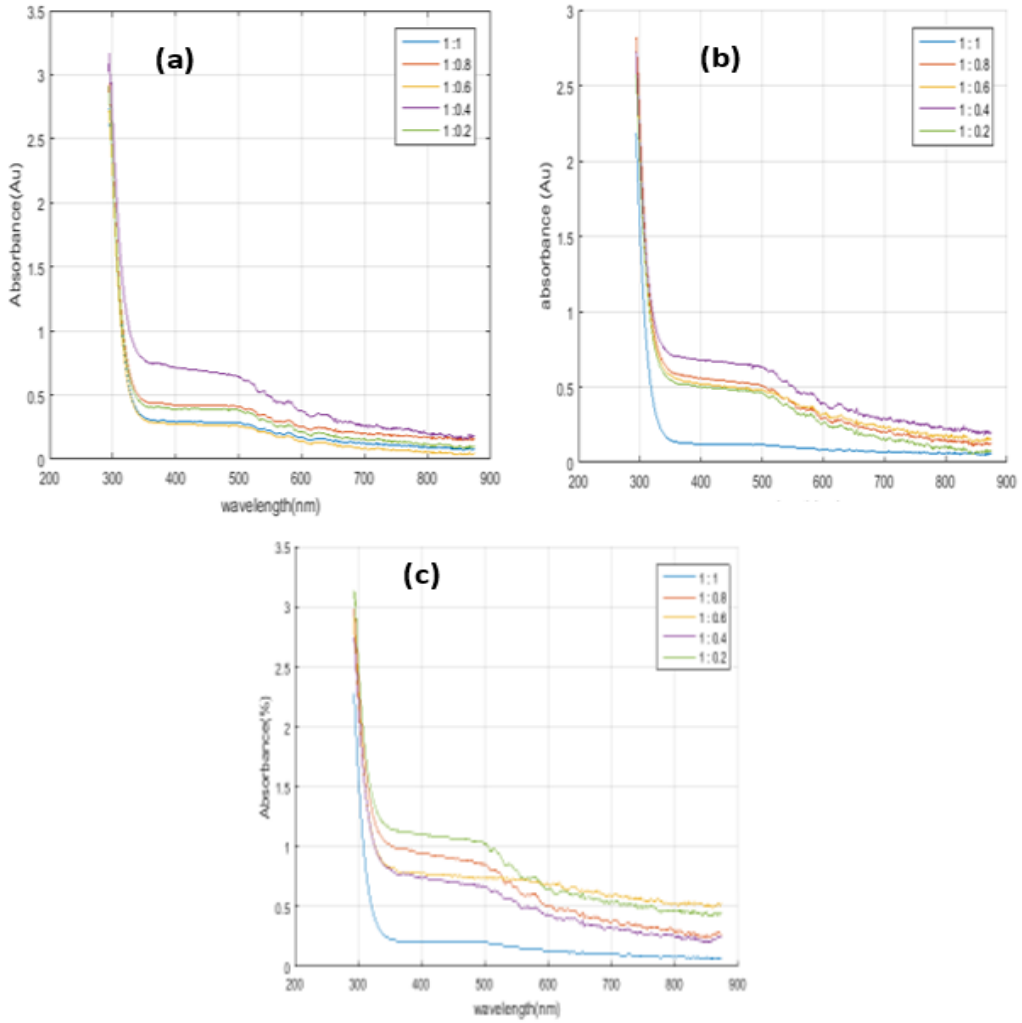

Figure 7. Absorbance Spectra of PANi/CuNP composites at a spin coating speed of (a) 1000 rpm (b) 2000 rpm, and (c) 3000 rpm.

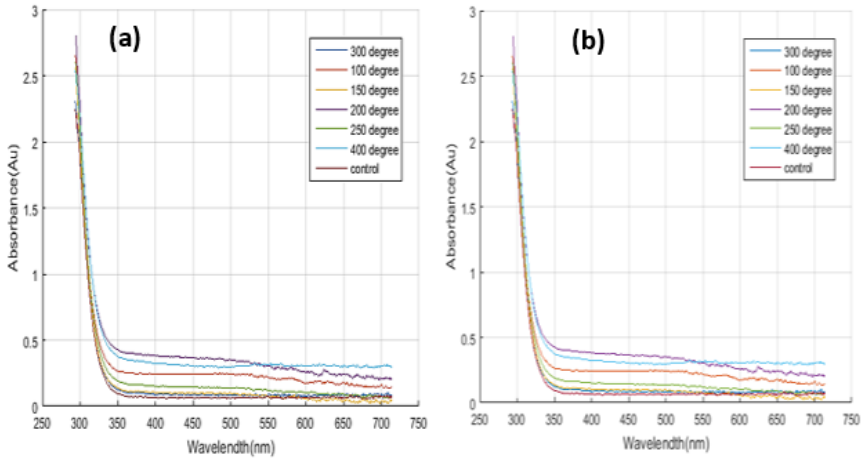

Figure 8. Absorbance Spectra of PANi/CuNP composites at different temperatures for (a) 30 Mins (b) 60 Mins.

From Figure 9, the value of the band gap was estimated by extrapolating the straight line at $(\alpha hv)^n = 0$, with n being the band gap transition-dependent exponent, allowed or forbidden, and either direct or indirect [43]. The band gap was calculated by plotting photon energy (hv) versus $(\alpha hv)^2$ (Figure 9). For the direct band gap transition of CuNP, n was taken

as 0.5 [44]. The band gap was obtained as 3.3 eV, which is in close agreement with that observed in previous studies [45–49]. The observed band gap value would greatly improve the photocatalytic behavior of this material.

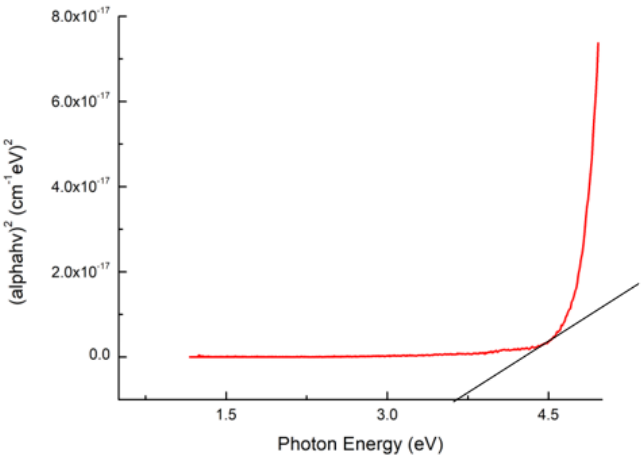

Figure 9. Plot of $(\alpha hv)^2$ versus photon energy (hv).

3.5. Photovoltaic performance.

The solar simulator measured the photovoltaic performance of the copper/Polymer fabricated solar cells (Agilent 4155C). The intensity of light during the measurement was 100 mW/cm^2. Figure 10 shows the I-V characteristics of the solar cells. The corresponding PV parameters, PCE (η), fill factor (FF), open-circuit voltage (V_{oc}), and current–density (Jsc), are listed in Table 1. These results showed that the PCE of the nanocomposites depends strongly on the amounts of CuNPs. PANI/CuNP(1:0.4) gives PCE of 19.201 %, which is higher than others and compares well with Si solar cells. This enhancement in efficiency could be attributed to an enhancement in the electrochemical activity at this mixing ratio.

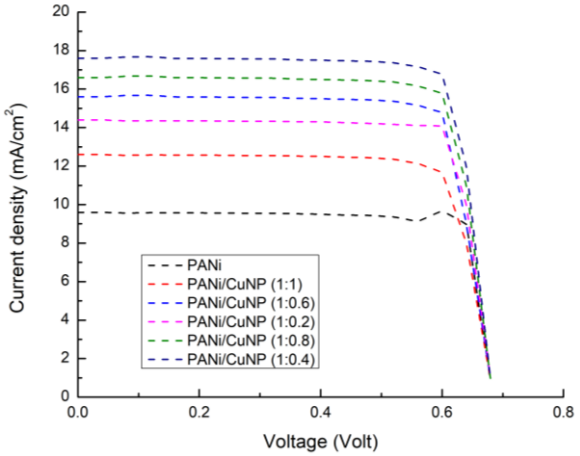

Figure 10. J-V characteristics of DSSCs based on PANi and PANi/CuNP composites.

Table 1. Photovoltaic performance of solar cell based on different Photo anodes.

Sample	CE	J_{SC} (mA/cm^{-2})	V_{OC}(v)	FF	PCE %
S1	PANI/CuNP(1:1)	12.72	0.635	0.858	17.921
S2	PANI/CuNP(1:0.8)	16.50	0.693	0.897	18.970
S3	PANI/CuNP(1:0.6)	15.60	0.684	0.890	18.910
S4	PANI/CuNP(1:0.4)	17.80	0.695	0.904	19.201
S5	PANI/CuNP(1:02)	14.20	0.658	0.892	18.950
S6	PANI	9.61	0.662	0.871	16.501

4. Conclusions

In this work, CuNPs were successfully synthesized. A simple approach using Siam Leaf extract as the reducing agent for synthesizing CuNPs has been reported. This approach eliminated the use of toxic chemicals for the synthesis of NPs. The synthesized CuNPs were characterized using various characterization techniques and further used to prepare nanocomposites for photovoltaic application. The I-V characteristics of the nanocomposites showed improved power conversion efficiency of 19.20 % conversion efficiency for PANI/40%CuNPs. Nanocomposite.

Funding

This research received no external funding.

Acknowledgments

The authors would also like to thank Dr. S.W. Balogun of the Material Science Research Laboratory, Kwara State University, Malete, Nigeria, for providing guidance during the material characterization.

Conflicts of Interest

The authors declare no conflict of interest.

References

1. Haque, A. Solar energy. In: *Electric Renewable Energy Systems.* Muhammad, H. Rashid Elsevier Inc. **2016**; pp. 40-59, https://doi.org/10.1016/B978-0-12-804448-3/00003-7.
2. De Brito, M.A.G.; Galotto, L.; Sampaio, L.P.; De Azevedo Melo, G.; Canesin, C.A. Evaluation of the main MPPT techniques for photovoltaic applications. *IEEE Trans. Ind. Electron.* **2013**, *60*, https://doi.org/10.1109/TIE.2012.2198036.
3. Martinez-Gracia, A. Solar energy availability. In: *Solar Hydrogen Production: Processes, Systems and Technologies.* Calise, F.; D'Accadia, M.D.; Santarelli, M.; Lanzini, A.; Ferrero, D. El Sevier Inc., **2019**; pp. 113-149, https://doi.org/10.1016/B978-0-12-814853-2.00005-9.
4. Mehmood, U.; Hussein, I.A.; Harrabi, K.; Tabet, N.; Berdiyorov, G.R. Enhanced photovoltaic performance with co-sensitization of a ruthenium(ii) sensitizer and an organic dye in dye-sensitized solar cells. *RSC Adv.* **2016**, *6*, https://doi.org/10.1039/c5ra26577k.
5. Karim, N.A.; Mehmood, U.; Zahid, H.F.; Asif, T. Nanostructured photoanode and counter electrode materials for efficient Dye-Sensitized Solar Cells (DSSCs). *Solar Energy* **2019**, *185*, 165-188, https://doi.org/10.1016/j.solener.2019.04.057.
6. Płaczek-Popko, E. Top PV market solar cells 2016. *Opto-Electronics Review* **2017**, *25*, 55-64, https://doi.org/10.1016/j.opelre.2017.03.002.
7. Mehmood, U.; Asghar, H.; Babar, F.; Younas, M. Effect of graphene contents in polyaniline/graphene composites counter electrode material on the photovoltaic performance of dye-sensitized solar cells (DSSCSs). *Solar Energy* **2020**, *196*, 132-136, https://doi.org/10.1016/j.solener.2019.12.024.
8. Huang, Y.; Luscombe, C.K. Towards Green Synthesis and Processing of Organic Solar Cells. *The Chemical Record* **2019**, *19*, 1039-1049, https://doi.org/10.1002/tcr.201800145.
9. Kheralla, A.; Chetty, N. A review of experimental and computational attempts to remedy stability issues of perovskite solar cells. *Heliyon* **2021**, *7*, https://doi.org/10.1016/j.heliyon.2021.e06211.
10. Mohd Yusoff, A.R.b.; Vasilopoulou, M.; Georgiadou, D.G.; Palilis, L.C.; Abate, A.; Nazeeruddin, M.K. Passivation and process engineering approaches of halide perovskite films for high efficiency and stability perovskite solar cells. *Energy & Environmental Science* **2021**, *14*, 2906-2953, https://doi.org/10.1039/D1EE00062D.
11. Mazumdar, S.; Zhao, Y.; Zhang, X. Stability of Perovskite Solar Cells: Degradation Mechanisms and Remedies, *Front. Electron.* **2021**, *2*, https://doi.org/10.3389/felec.2021.712785.

12. Qiu, L.; Ono, L.K.; Qi, Y. Advances and challenges to the commercialization of organic–inorganic halide perovskite solar cell technology. *Materials Today Energy* **2018**, *7*, 169-189, https://doi.org/10.1016/j.mtener.2017.09.008.
13. Siddika, A.; Sultana, M.; Bashar, M.S.; Tabassum, S.; Aziz, S.; Ali Shaikh, M.A. Improved performance of dye sensitized solar cell by exploration of photoanode and ruthenium based dye. *Optical Materials* **2022**, *125*, https://doi.org/10.1016/j.optmat.2022.112042.
14. Haran, N.H.; Yousif, Q.A. The efficiency of TiO2 nanotube photoanode with graphene nanoplatelets as counter electrode for a dye-sensitised solar cell. *International Journal of Ambient Energy* **2022**, *43*, 336-343, https://doi.org/10.1080/01430750.2019.1636880.
15. Baby, R.; Nixon, P.D.; Kumar, N.M.; Subathra, M.S.P.; Ananthi, N. A comprehensive review of dye-sensitized solar cell optimal fabrication conditions, natural dye selection, and application-based future perspectives. *Environmental Science and Pollution Research* **2022**, *29*, 371-404, https://doi.org/10.1007/s11356-021-16976-8.
16. Kim, J.-H.; Kim, D.-H.; So, J.-H.; Koo, H.-J. Toward Eco-Friendly Dye-Sensitized Solar Cells (DSSCs): Natural Dyes and Aqueous Electrolytes. *Energies* **2022**, *15*, https://doi.org/10.3390/en15010219.
17. Li, Y.; Zhang, W.; Li, X.; Xu, Y. Boosting the photoelectric conversion efficiency of DSSCs through graphene quantum dots: insights from theoretical study. *Materials Chemistry Frontiers* **2021**, *5*, 5814-5825, https://doi.org/10.1039/d1qm00580d.
18. Iwata, S.; Shibakawa, S.-i.; Imawaka, N.; Yoshino, K. Stability of the current characteristics of dye-sensitized solar cells in the second quadrant of the current–voltage characteristics. *Energy Reports* **2018**, *4*, 8-12, https://doi.org/10.1016/j.egyr.2017.10.004.
19. Akman, E. Enhanced photovoltaic performance and stability of dye-sensitized solar cells by utilizing manganese-doped ZnO photoanode with europium compact layer. *Journal of Molecular Liquids* **2020**, *317*, https://doi.org/10.1016/j.molliq.2020.114223.
20. Esgin, H.; Caglar, Y.; Caglar, M. Photovoltaic performance and physical characterization of Cu doped ZnO nanopowders as photoanode for DSSC. *J. Alloys Compd.* **2022**, *890*, https://doi.org/10.1016/j.jallcom.2021.161848.
21. Grätzel, M. Solar Energy Conversion by Dye-Sensitized Photovoltaic Cells. *Inorganic Chemistry* **2005**, *44*, 6841-6851, https://doi.org/10.1021/ic0508371.
22. Lee, C.-P.; Li, C.-T.; Ho, K.-C. Use of organic materials in dye-sensitized solar cells. *Materials Today* **2017**, *20*, 267-283, https://doi.org/10.1016/j.mattod.2017.01.012.
23. Bae, J.-H.; Do, S.-B.; Cho, S.-H.; Lee, K.-M.; Lee, S.-E.; Kim, T.-O. TiO2 treatment using ultrasonication for bubble cavitation generation and efficiency assessment of a dye-sensitized solar cell. *Ultrasonics Sonochemistry* **2022**, *83*,https://doi.org/10.1016/j.ultsonch.2022.105933.
24. Reddy, N.P.; Santhosh, R.; Thogiti, S.; Muniramaiah, R.; Joseph, D.P.; Murali, B. Nanostructured ternary perovskite oxides as photoconversion efficiency enhancers for DSSC. *Journal of Materials Chemistry C* **2022**, *10*, 1403-1413, https://doi.org/10.1039/d1tc04584a.
25. Schoden, F.; Dotter, M.; Knefelkamp, D.; Blachowicz, T.; Schwenzfeier Hellkamp, E. Review of State of the Art Recycling Methods in the Context of Dye Sensitized Solar Cells. *Energies* **2021**, *14*, https://doi.org/10.3390/en14133741.
26. T. Önen, T.;Karakuş, M.Ö.; Coşkun, R.; Çetin, H. Reaching stability at DSSCs with new type gel electrolytes. *J. Photochem. Photobiol. A Chem.* **2019**, *385*, https://doi.org/10.1016/j.jphotochem.2019.112082.
27. Muchuweni, E.; Martincigh, B.S.; Nyamori, V.O. Recent advances in graphene-based materials for dye-sensitized solar cell fabrication. *RSC Advances* **2020**, *10*, 44453-44469, https://doi.org/10.1039/d0ra08851j.
28. Hiragino, Y.; Tanaka, T.; Takeuchi, H.; Takeuchi, A.; Lin, J.; Yoshida, T.; Fujita, Y. Synthesis of nitrogen-doped ZnO nanoparticles by RF thermal plasma. *Solid-State Electronics* **2016**, *118*, 41-45, https://doi.org/10.1016/j.sse.2016.01.003.
29. Tseng, K.-H.; Chou, C.-J.; Liu, T.-C.; Haung, Y.-H.; Chung, M.-Y. Preparation of Ag-Cu Composite Nanoparticles by the Submerged Arc Discharge Method in Aqueous Media. *Materials Transactions* **2016**, *57*, 294-301, https://doi.org/10.2320/matertrans.M2015288.
30. Benelmekki, M.; Vernieres, J.; Kim, J.-H.; Diaz, R.-E.; Grammatikopoulos, P.; Sowwan, M. On the formation of ternary metallic-dielectric multicore-shell nanoparticles by inert-gas condensation method. *Materials Chemistry and Physics* **2015**, *151*, 275-281, https://doi.org/10.1016/j.matchemphys.2014.11.066.
31. Mafuné, F.; Kohno, J.-y.; Takeda, Y.; Kondow, T.; Sawabe, H. Formation of Gold Nanoparticles by Laser Ablation in Aqueous Solution of Surfactant. *The Journal of Physical Chemistry B* **2001**, *105*, 5114-5120, https://doi.org/10.1021/jp0037091.
32. Kawasaki, M.; Nishimura, N. 1064-nm laser fragmentation of thin Au and Ag flakes in acetone for highly productive pathway to stable metal nanoparticles. *Applied Surface Science* **2006**, *253*, 2208-2216, https://doi.org/10.1016/j.apsusc.2006.04.024.
33. Pal, S.; Tak Yu, K.; Song Joon, M. Does the Antibacterial Activity of Silver Nanoparticles Depend on the Shape of the Nanoparticle? A Study of the Gram-Negative Bacterium Escherichia coli. *Applied and Environmental Microbiology* **2007**, *73*, 1712-1720, https://doi.org/10.1128/AEM.02218-06.

34. Tarasenko, N.V.; Butsen, A.V.; Nevar, E.A.; Savastenko, N.A. Synthesis of nanosized particles during laser ablation of gold in water. *Applied Surface Science* **2006**, *252*, 4439-4444, https://doi.org/10.1016/j.apsusc.2005.07.150.
35. Pal, G.; Rai, P.; Pandey, A. Chapter 1 - Green synthesis of nanoparticles: A greener approach for a cleaner future. In: *Green Synthesis, Characterization and Applications of Nanoparticles*. Shukla, A.K.; Iravani, S. Eds.; Elsevier: **2019**; pp. 1-26, https://doi.org/10.1016/b978-0-08-102579-6.00001-0.
36. Mansor, M.R.; Mustafa, Z.; Fadzullah,S.H.S.M.; Omar, G; Salim, M.A.; Akop, M.Z. *Recent Advances in Polyethylene-Based Biocomposites.* In: *Natural Fibre Reinforced Vinyl Ester and Vinyl Polymer Composites*. Sapuan, S.M.; Ismail, H.; Zainudin, E.S. Eds.; Woodhead Publishing: **2018**; pp. 71-96, https://doi.org/10.1016/b978-0-08-102160-6.00003-2.
37. Ingham, B.; Toney, M.F. 1 - X-ray diffraction for characterizing metallic films. In: *Metallic Films for Electronic, Optical and Magnetic Applications*. Barmak, K.; Coffey, K. Eds.; Woodhead Publishing: **2014**; pp. 3-38, https://doi.org/10.1533/9780857096296.1.3.
38. Tamayo, L.; Azócar, M.; Kogan, M.; Riveros, A.; Páez, M. Copper-polymer nanocomposites: An excellent and cost-effective biocide for use on antibacterial surfaces. *Mater. Sci. Eng. C* **2016**, *69*, 1391–1409, https://doi.org/10.1016/j.msec.2016.08.041.
39. Guillén, E.; Azaceta, E.; Vega-Poot, A.; Idígoras, J.; Echeberría, J.; Anta, J.A.; Tena-Zaera, R. ZnO/ZnO Core–Shell Nanowire Array Electrodes: Blocking of Recombination and Impressive Enhancement of Photovoltage in Dye-Sensitized Solar Cells. *The Journal of Physical Chemistry C* **2013**, *117*, 13365-13373, https://doi.org/10.1021/jp402888y.
40. Al-Saadi, T.M.; Hussein, B.H.; Hasan, A.B.; Shehab, A.A. Study the Structural and Optical Properties of Cr doped SnO2 Nanoparticles Synthesized by Sol-Gel Method. *Energy Procedia* **2019**, *157*, 457-465, https://doi.org/10.1016/j.egypro.2018.11.210.
41. Themlin, J.M.; Sporken, R.; J. Darville, J.; R. Caudano, R.; Gilles, J.M. Resonant-photoemission study of SnO2: Cationic origin of the defect band-gap states. *Physical Review B* **1990**, *42*, 11914-11925, https://doi.org/10.1103/physrevb.42.11914.
42. Omar, M.A. *Elementary Solid State Physics: Principles and Applications*. 2nd edition, Addison Wesley Publishing Company **1993**.
43. Jbara, A.S.; Othaman, Z.; Saeed, M.A. Structural, morphological and optical investigations of θ-Al2O3 ultrafine powder'. *J. Alloys Compd.* **2017**, *718*, 1–6, https://doi.org/10.1016/j.jallcom.2017.05.085.
44. D. A. Dholakia, D.ASolanki, G.K.; Patel, S.G.; Agarwal, M.K. Optical band gap studies of tungsten sulphoselenide single crystals grown by a DVT technique. *Scientia Iranica* **2003**, *10*, 373–382.
45. Sagadevan, S. Analysis of Structure, Surface Morphology, Optical and Electrical Properties of Copper Nanoparticles. *J. Nanomedicine Res.* **2015**, *2*, 133–136, https://doi.org/10.15406/jnmr.2015.02.00040.
46. Mohindroo, J.J.; Garg, U.K.; Sharma, A.K. Optical properties of stabilized copper nanoparticles. *AIP Conf. Proc.* **2016**, *1728*, https://doi.org/10.1063/1.4946585.
47. Tito, I.A.; Uddin, S.; Islam, S.; Bhowmik, S. Copper Nanoparticle(CuNP's)Synthesis: A review of the various ways with Photocatalytic and Antibacterial Activity. *Orient. J. Chem.* **2021**, *37*, https://doi.org/10.13005/ojc/370503.
48. Sharaf Zeebaree, S.Y.; Sharaf Zeebaree, A.Y.; Haji Zebari, O.I.; Sharaf Zebari, A.Y. Sustainable fabrication, optical properties and rapid performance of bio-engineered copper nanoparticles in removal of toxic methylene blue dye in an aqueous medium. *Curr. Res. Green Sustain. Chem*. **2021**, *4*, https://doi.org/10.1016/j.crgsc.2021.100103.
49. Selvanathan, V.; Aminuzzaman, M.; Tey, L.; Razali, S.A.; Althubeiti, K.; Alkhammash, H.I.; Guha, S.K.; Ogawa, S.; Watanabe, A.; Shahiduzzaman, M.; Akhtaruzzaman, M. Muntingia calabura leaves mediated green synthesis of cuo nanorods: Exploiting phytochemicals for unique morphology, *Materials* **2021**, *14*, https://doi.org/10.3390/ma14216379.